Friction Compensation in a Controlled One-Link Robot Using a Reduced-Order Observer

Niels Mallon, Nathan van de Wouw, Devi Putra, and Henk Nijmeijer, *Fellow, IEEE*

***Abstract*—In this paper, friction compensation in a controlled one-link robot is studied. Since friction is generally velocity dependent and controlled mechanical systems are often equipped with position sensors only, friction compensation requires some form of velocity estimation. Here, the velocity estimate is provided by a reduced-order observer. The friction is modeled by a set-valued velocity map including an exponential Stribeck curve. For the resulting discontinuous closed-loop dynamics, both the case of exact friction compensation and nonexact friction compensation are investigated. For the case of exact friction compensation, design rules in terms of controller and observer parameter settings, guaranteeing global exponential stability of the set-point are proposed. If the proposed design rules are not fulfilled, the system can exhibit a nonzero steady-state error and limit cycling. Moreover, in the case of nonexact friction compensation, it is shown that undercompensation leads to the existence of an equilibrium set and overcompensation leads to limit cycling. These results are obtained both numerically and experimentally.**

***Index Terms*—Asymptotic stability, compensation, discontinuities, friction, limit cycles, observers, switching systems.**

I. Introduction

THE presence of dry friction in controlled mechanical systems concerning a positioning task, can give rise to undesired effects, such as large steady-state errors, large settling times, and stick-slip behavior [1]–[4]. A common approach to attain high performance for such systems is to apply model-based friction compensation. Indeed, already, many friction compensation approaches are available (see, for example, [1]–[3], [6], [7], and [9]–[11]). In these references, friction compensation is investigated in both a feedforward manner (the friction compensation is based on the desired variables) and a feedback manner (the friction compensation is based on the actual variables). For a more complete overview of possible variants of friction beating strategies and their merits, we refer to the references [1], [2], [9]. Here, we will apply a feedback model based friction compensation strategy to a one-link robot in order to enhance its positioning accuracy. The model-based friction compensation approach, as discussed in this paper, distinguishes itself from other already available model-based friction compensation techniques by the fact that it includes an *observer* to estimate the actual velocity from position measurements (no velocity sensors are needed), the incorporated discontinuous model of the friction captures known friction phenomena like stiction and an exponentially Stribeck curve, and it is supported by design rules in closed form which guarantee global exponential stability (GES) of the resulting closed-loop system.

In general, a proportional-derivative (PD) controller with an additional integral action (I) on the position error is used for steady-state positioning control of mechanical systems with friction. However, the integral action in the controller in combination with descending slope of the friction around zero velocity can cause instability (also known as *hunting* [2], [3]). Since we want to focus only to possible instabilities caused by the additional observer dynamics in model-based friction compensation and to keep the analysis as simple as possible, only a linear PD position controller is considered in this paper. However, some results can easily be extended for other controllers, for example PI or PID controllers. Based on experiments, a model of the friction depending on velocity is adopted here. The model is a set-valued friction law including the Stribeck effect. Clearly, such a model does not capture dynamical friction phenomena [7], [8], essential for certain control tasks with friction compensation, for example, tracking with velocity reversals at very slow velocities [15]. However, depending on the application, the dynamical friction effects may be neglected by applying friction compensation based on relatively simple friction models which require less parameters to identify and are easier to incorporate in a real-time environment.

Since only position measurements are available for the one-link robot (and for controlled mechanical systems in general), some form of velocity estimation is required. To this end, an observer can be used (see, for example, [12], [13], [15]). The combination of dry friction, friction compensation, and the observer dynamics can give rise to undesired phenomena, such as steady-state positioning errors and limit cycling [13]. In [13], a friction compensation strategy combined with a PD controller, based on a full-order observer and a static friction model, is studied, and it is shown that such limit cycling can be avoided for certain parameter settings of the controller and the observer. However, the origin of the limit cycling behavior is still not fully understood and design rules regarding the controller and observer parameters, to avoid undesired equilibrium sets and limit cycling are not provided. In this paper, friction compensation based on a reduced-order observer (formerly known as a reduced dimension observer [14]) is studied. In contrast to a full-order observer, a reduced-order observer estimates only those states which are not directly measured.

The application of a reduced-order observer for the estimation of the velocity of the one-link robot, using the position measurements, implies first-order observer dynamics with only a single design parameter. In [15], friction compensation based on a dynamical friction model and a reduced-order observer is

Manuscript received May 17, 2004. Manuscript received in final form December 8, 2005. Recommended by Associate Editor F. Ghorbel. This work was performed while D. Putra was with the Eindhoven University of Technology.

N. Mallon, N. van de Wouw, and H. Nijmeijer are with the Dynamics and Control Group, Department of Mechanical Engineering, Eindhoven University of Technology, 5600 MB Eindhoven, The Netherlands.

D. Putra is with the Control Theory and Applications Centre, Coventry University, CV1 5ED, U.K.

Digital Object Identifier 10.1109/TCST.2005.863674

applied successfully for a tracking control problem. However, a rigorous stability analysis of the resulting closed-loop system is not performed and design rules are not provided.

For the combination of controller and observer as studied in this paper, a rigorous stability analysis is performed for the case of exact friction compensation. This stability analysis results in design rules for the parameters of the controller and observer, such that GES of the set point is guaranteed. Clearly, these design rules guarantee that nonzero steady-state errors and limit cycling are avoided. This analysis is performed by separating the (nonlinear) observer error dynamics and the system dynamics, analogous to the separation principle as known for linear systems [18]. The systematic approach proposed here can be applied for other controllers and may be extended for multi-degree-of-freedom systems with both full-order and reduced-order observers.

In practice, small friction modeling errors can not be avoided. These friction modeling errors may induce some level of overcompensation or undercompensation of the friction. In [10] and [17], limit cycling due to overcompensation of the friction based on sensed velocity is reported. For a tracking control problem, friction modeling errors are related in [16] to observed oscillatory responses (especially at velocity reversals) in the case of feedforward friction compensation and to zero velocity intervals in the case of disturbance-observer based compensation due to delays in the response of the applied disturbance observer. In [15], it is shown in simulation that neglecting dynamical friction effects in model based friction compensation based on sensed velocity may lead to undesirable oscillations at velocity reversals. To our knowledge, no results are present on the effect of small friction modeling errors for observer-based friction compensation strategies incorporated in a steady-state positioning task controller. In this paper, we study the effect of small friction modeling errors on the proposed observer-based friction compensation strategy by numerical means and the results are validated with experiments.

The paper is organized as follows. First, the modeling and identification of the one-link robot, based on experiments, will be discussed in Section II. Next, in Section III, the controller design, observer design and the adopted friction compensation strategy are discussed. Section IV concerns the analysis of the dynamic behavior of the system in the case of exact friction compensation. This analysis results in design rules for the controller and observer such that GES of the set point is guaranteed. The consequences of (small) friction modeling errors on the dynamic behavior of the system are investigated in Section V and the results are validated with experiments in Section VI. Finally, in Section VII, conclusions are presented.

II. Experimental Setup, Modelling, and Identification

The system under consideration is a controlled one-link robot. From previous research [3], it is known that the positioning behavior of this setup suffers largely from the presence of dry friction. This one-link robot is, therefore, a good carrier for the research on the proposed friction compensation strategy to ensure accurate positioning. The robot is modeled as a single inertia J (modeling the inertia of both the driveline and the link) subjected to a viscous friction torque $-b\dot{q}$, a dry friction torque

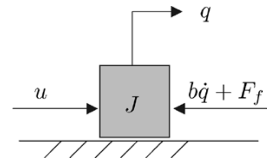

Fig. 1. Schematical representation of the one-link robot.

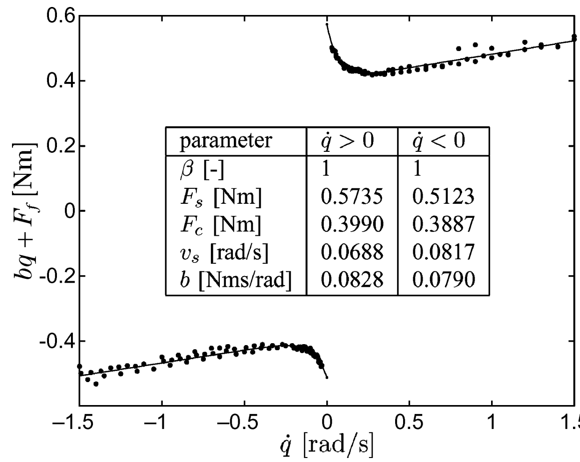

Fig. 2. (Dots) Friction measurements versus (solid line) friction model and identified parameters.

$-F_f$, and a motor torque u (see Fig. 1). These assumptions lead to the following model for the one-link robot:

$$J\ddot{q} = u - b\dot{q} - F_f(\dot{q}). \tag{1}$$

Using a frequency-domain identification technique, the total inertia of the system is identified to be $J = 0.026\,\text{kgm}^2/\text{rad}$ [3]. In order to measure the friction-velocity map, break-away experiments are performed to measure the static friction torque and constant velocity experiments are performed to measure the friction-velocity map at nonzero (constant) velocities. In these measurements, the Stribeck effect is evident and must be included in the dry friction model, see Fig. 2. The dry friction model is expressed as a set-valued force law by the following algebraic inclusion:

$$F_f(v) \in \begin{cases} g^+(v), & \text{if } v > 0 \\ -g^-(v), & \text{if } v < 0 \\ [-F_s^-, F_s^+], & \text{if } v = 0 \end{cases} \tag{2}$$

with $g^+(v)$ and $g^-(v)$ the Stribeck curve for positive and negative velocity, respectively. The set-valued nature of (2) at $v = 0$ allows to model the stiction phenomena. The Stribeck curve is defined by the exponential curve (here, for $v > 0$, indicated by the superscript "+")

$$g^+(v) = F_c^+ + \delta F^+ e^{-\left(\frac{|v|}{v_s^+}\right)^{\beta^+}} \tag{3}$$

where F_c^+ is the Coulomb friction torque, F_s^+ is the static friction torque, δF^+ is the difference between the static and Coulomb friction torque ($\delta F^+ = F_s^+ - F_c^+$), v_s^+ is the Stribeck velocity, and β^+ is the Stribeck shape parameter; for $v < 0$, these parameters are indicated by the superscript "$-$." The friction model (2) allows for an asymmetric friction curve to

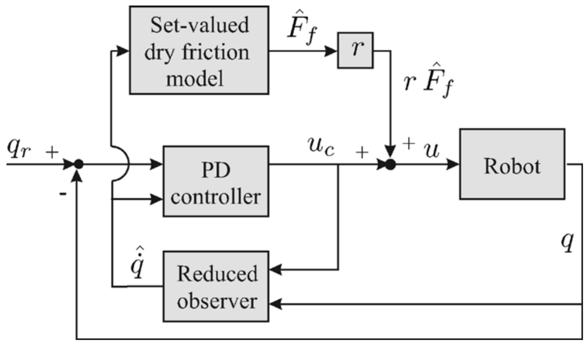

Fig. 3. Friction compensation strategy.

ensure an accurate fit of the measured friction characteristics, see Fig. 2. The values of the friction parameters are obtained by fitting the Stribeck curve (3) with the viscous friction term $-b\dot{q}$ to the friction measurement data for both positive and negative velocities separately. The fit and the estimates of the friction parameters are also depicted in Fig. 2. The asymmetry in the dry friction is significant and is taken into account. However, since we want to consider only a (smooth) linear reduced-order observer, the asymmetry for the viscous friction is not taken into account in the observer design, see Section II. For that purpose only, the viscous friction coefficient is set to the average value $(b^+ + b^-)/2 = 0.0809$ [Nms/rad].

III. Closed-Loop System Design

The combination of the PD controller and friction compensation, incorporating a reduced-order observer, as applied to the one-link robot is depicted schematically in Fig. 3. The total motor torque $u = u_c + u_{fc}$ is composed by a feedback controller torque u_c and the friction compensation torque u_{fc}. The controller torque is defined by

$$u_c = n_1(q_r - q) - n_2\hat{\dot{q}} \tag{4}$$

where $n_1, n_2 > 0$ are the proportional gain and the derivative gain, respectively, and $\hat{\dot{q}}$ the velocity estimate provided by the observer. Without loss of generality, the desired position q_r will be assumed to equal zero. Furthermore, the following set-valued friction compensation law, analogous to (2), is adopted:

$$u_{fc} = rF_f(\hat{\dot{q}}) \tag{5}$$

with r a scaling factor of the friction compensation and $F_f(\cdot)$ defined by (2). Clearly, u_{fc} reflects a feedback compensation strategy based on an estimated velocity provided by an observer. When $r = 1$, exact friction compensation is attained, when $r \neq 1$ nonexact friction compensation is attained. The adopted friction compensation law (5) is set valued for $\hat{\dot{q}} = 0$. Of course in practice one can only implement a specific compensation torque at $\hat{\dot{q}} = 0$. In Appendix I, it is shown that under the proposed design rules, uniqueness of solutions is guaranteed for the closed-loop system as depicted in Fig. 3. Consequently, in practice, any single-valued compensation torque taken from the set $r[-F_s^-, F_s^+]$ suffices to compensate the friction for $\hat{\dot{q}} = 0$.

The linear reduced-order observer reads as

$$\dot{\hat{\dot{q}}} = -\frac{b}{J}\hat{\dot{q}} + \frac{1}{J}u_c + L(\dot{q} - \hat{\dot{q}}) \tag{6}$$

where $\hat{\dot{q}}$ is the observer state (the velocity estimate) and $L > 0$ the observer gain. In (6), a model-based part $(-(b/J)\hat{\dot{q}} + (1/J)u_c)$ and a linear injection term $(L(\dot{q} - \hat{\dot{q}}))$ can be recognized. To avoid the difficulty that (6) still depends on the unmeasured velocity $\dot{q}$, a new observer state [18] is defined: $z = \hat{\dot{q}} - Lq$. In terms of this new state, the reduced-order observer (6) reads as $\dot{z} = -((b + LJ)/J)(z + Lq) + (1/J)u_c$, in which only the measured angular position q appears. The reduced-order observer in the latter form is only provided for implementation purposes, the analysis in this paper will use the formulation of as in (6). The observer error is defined as $e = \dot{q} - \hat{\dot{q}}$, and its dynamics obey the following scalar differential inclusion:

$$\dot{e} = \ddot{q} - \dot{\hat{\dot{q}}} \in -\frac{b + LJ}{J}e + \frac{rF_f(\hat{\dot{q}}) - F_f(\dot{q})}{J} \tag{7}$$

which can clearly be influenced by the observer gain L for $e \neq 0$. Adopting the state coordinates $\mathbf{x} = [q\ \hat{\dot{q}}\ e]^T \equiv [x_1\ x_2\ x_3]^T$, the dynamics of the closed-loop system, as depicted in Fig. 3, can be formulated by the following differential inclusion:

$$\begin{aligned}
\dot{x}_1 &= x_2 + x_3\\
\dot{x}_2 &= -\frac{n_1}{J}x_1 - \frac{b + n_2}{J}x_2 + Lx_3\\
\dot{x}_3 &\in -\frac{b + LJ}{J}x_3 + \frac{1}{J}\left(rF_f(x_2) - F_f(x_2 + x_3)\right).
\end{aligned} \tag{8}$$

The differential inclusion (8) is of Filippov-type, and Filippov's solution concept [20] can be adopted. Consequently, the existence of solutions for (8) is guaranteed. However, uniqueness of solutions is not automatically guaranteed. In the Appendix I, it is shown that uniqueness of solutions of (8) can only be guaranteed if $r \leq 1$ and

$$L + \frac{n_1}{L} > \frac{1}{J}(-\lambda - b) \tag{9}$$

where $\lambda = \min_{x \in \mathbb{R}\setminus\{0\}}[(\partial g^+(x)/\partial x), (\partial g^-(x)/\partial x)]$ is the maximum rate of decay of the friction model (2), defined by

$$\lambda = \min\left(-\frac{\eta^+\delta F^+}{v_s^+}, -\frac{\eta^-\delta F^-}{v_s^-}\right) \tag{10}$$

and

$$\eta^i = \begin{cases} 1, & \text{if } \beta^i = 1\\ \dfrac{(\beta^i - 1)e^{-\frac{\beta^i - 1}{\beta^i}}}{\beta^i\sqrt[\beta^i]{\frac{\beta^i - 1}{\beta^i}}}, & \text{if } \beta^i > 1 \end{cases}. \tag{11}$$

Under this condition, the solution of (8) is not influenced by which exact value of the friction compensation torque is taken for $\hat{\dot{q}} = 0$ from the set $r[-F_s^-, F_s^+]$. This property is beneficial for implementation purposes.

IV. Exact Friction Compensation

In this section, the behavior of the closed-loop system (8) is investigated for the case of exact friction compensation $(r = 1)$.

First, the existence of an equilibrium set, and its dependence on the design variables, is discussed. Next, the stability of the set-point (the origin) is investigated.

A. Equilibrium Set

It is important to study the equilibria of (8) and their dependencies on the design variables. After all the closed-loop system concerns, a positioning task and equilibria other than the origin represent a state of nonzero steady-state error. Equilibria of (8), denoted by $\mathbf{x}^*$, must satisfy the following equations and inclusion:

$$x_2^* = -x_3^* \tag{12}$$

$$x_1^* = -\frac{b + LJ + n_2}{n_1} x_2^* \tag{13}$$

$$G(x_2^*) \in \left[-F_s^-, F_s^+\right] \tag{14}$$

where $G(x) = (b + LJ)x + F_f(x)$. Clearly, the origin is always an equilibrium, as desired. However, depending on the observer gain L, an equilibrium set exists. In Fig. 4, the equilibria of the system with exact compensation are compared to those of the system with no compensation. In Fig. 4, the effect of the existence of the equilibrium set on the steady-state position error x_1 is depicted for $n_1 = 0.4$, $n_2 = 0.02$ and for varying L. The use of friction compensation ensures a significant decrease in the size of the equilibrium set. Moreover, in the case of exact friction compensation, the equilibrium set shrinks to an isolated equilibrium point for increasing observer gain at some critical value for the observer gain. In order to derive the condition for L such that a single equilibrium point exists, we note that $\lim_{x \downarrow 0} G(x) = F_s^+$ and $\lim_{x \uparrow 0} G(x) = -F_s^-$. Taking into account the strictly decreasing nature of $F_f(x)$ for $x \neq 0$, a sufficient and necessary condition, under which no equilibrium set can exist, is that $G(x)$ is strictly increasing for all $x \neq 0$ [see inclusion (14)]. This is attained if $(\partial/\partial x)G(x) > 0 \forall x \neq 0$ and, consequently, if

$$L > \frac{1}{J}(-\lambda - b) = L_c \tag{15}$$

with λ defined by (10). For the (asymmetric) parameters of the model of the one-link robot, the critical observer gain for negative velocity is $L_c^- = 55.07$ and for positive velocity is $L_c^+ = 94.4$. Consequently, the critical observer gain follows in this case from the parameters for positive velocity: $L_c = 94.4$. Note that the observer gain values at which the positive and the negative side of the equilibrium set in Fig. 4 disappears correspond to the values for L_c^- and L_c^+, respectively. The relation between the controller gains and the size of the equilibrium set (and the corresponding maximum steady-state positioning error) follows from (13); if n_1 is increased, the size of the equilibrium set decreases, and if n_2 is increased, the size of the equilibrium set increases.

B. Stability of the Closed-Loop System

Conditions for the combination of controller and observer gain(s) for which GES of the origin of (8) is guaranteed are of great importance. Namely, if GES of the origin can be attained, the absence of undesired steady-state errors and limit cycling

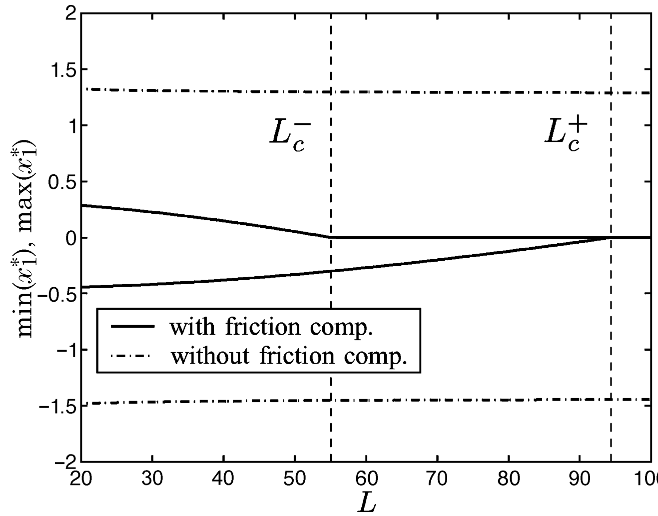

Fig. 4. Bounds for steady-state position error depending on L for $n_1 = 0.4$ and $n_2 = 0.02$.

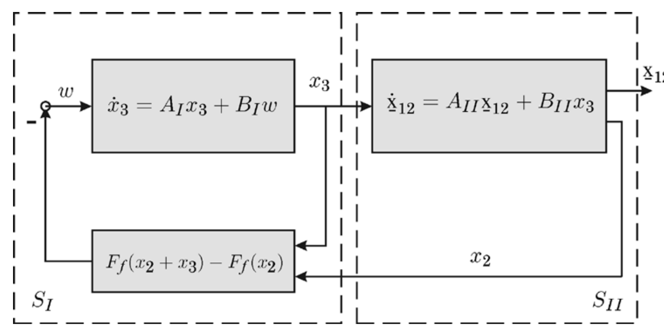

Fig. 5. Cascade representation of the closed-loop system.

is guaranteed. In order to investigate the stability of the origin of (8), we note that the system can be studied in the form of a cascade of two subsystems S_I and S_{II}, as depicted in Fig. 5. In this figure, $\mathbf{x}_{12} = [x_1\ x_2]^T$, and the system and input matrices of these subsystems are given by $A_I = -(b + LJ)/J$, $B_I = 1/J$ and

$$A_{II} = \begin{bmatrix} 0 & 1 \\ -\frac{n_1}{J} & -\frac{b+n_2}{J} \end{bmatrix}, \quad B_{II} = \begin{bmatrix} 1 \\ L \end{bmatrix}.$$

In order to prove the GES of the origin of (8), we adopt the following reasoning if the following three conditions are fulfilled:

a) the subsystem S_{II} is input-to-state stable (ISS) [21];
b) $\mathbf{x}_{12} = \mathbf{0}$ is a globally exponential stable equilibrium of the subsystem S_{II} for zero input x_3;
c) $x_3 = 0$ is a globally exponentially stable equilibrium point of the subsystem S_I for all x_2.

Then, $\mathbf{x} = \mathbf{0}$ is a globally exponentially stable equilibrium point of (8).[1] Let us now check when these conditions are fulfilled. First, conditions a) and b) are satisfied since system S_{II} is a LTI-system with a Hurwitz system matrix A_{II} and a bounded input matrix B_I (A_{II} is Hurwitz given the fact that $b, n_1, n_2 >$

[1]Note that the application of a other type of controller, such as a PI or PID controller, only affects the subsystem S_{II}. The extension of the proposed approach for other type of controllers is, therefore, straightforward.

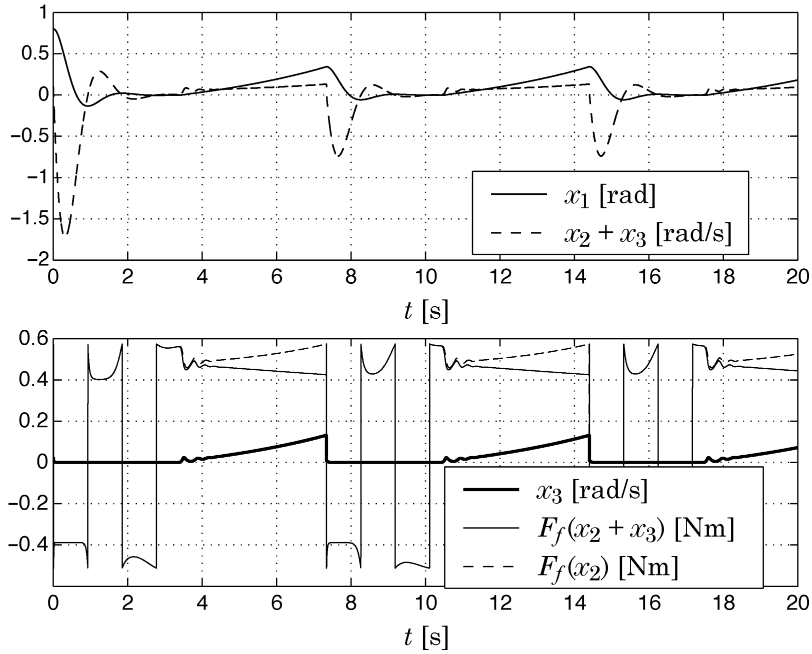

Fig. 6. Limit cycle for $n_1 = 0.4$, $n_2 = 0.02$, $L = 40 < L_c$, and $r = 1$ (simulation).

0). Before we check condition c), it is emphasized that S_I describes the observer error dynamics (7). Consequently, condition c) requires the stability of the observer error e. In order to investigate the stability of the observer error, we use a candidate Lyapunov function $V = (1/2)x_3^2$ (see [20] and [22] for details on Lyapunov analysis for differential inclusions). Its time derivative $\dot{V} = x_3\dot{x}_3$ obeys

$$\dot{V} \in -\frac{b+LJ}{J}x_3^2 + \frac{1}{J}\left(F_f(x_2) - F_f(x_2+x_3)\right)x_3. \quad (16)$$

In the second term of $\dot{V}$, the discontinuities of both the dry friction torque and the friction compensation law are present. Here, we will estimate this term by realizing that the function $F_f(\cdot)$ satisfies the following incremental sector condition:

$$\lambda x_3^2 \leq \left(F_f(x_2+x_3) - F_f(x_2)\right)x_3 \; \forall\, x_2, x_3 \quad (17)$$

with λ defined by (10). Using (17) in (16) yields $\dot{V} \leq -(b/L + J + \lambda/J)x_3^2 = -2(b/L + J + \lambda/J)V$. Clearly, for an observer gain satisfying $L > L_c$ with the critical observer gain L_c given by (15), the observer error is globally exponentially stable (independent of x_2) and condition c) is fulfilled.

Summarizing, we can conclude that for $L > L_c$, $\mathbf{x} = \mathbf{0}$ is a globally exponentially stable equilibrium point of (8) for all n_1, $n_2 > 0$. Note that for $L > L_c$, (9) is also fulfilled and solutions are, therefore, also guaranteed to be unique for $L > L_c$.

If $L < L_c$, undesired behavior in the form of a steady-state error (see Fig. 4) or limit cycling (see Fig. 6) can occur. The latter figure indicates that $e = 0$ is not stable for this observer gain value, which causes a nonzero observer error. The nonzero observer error induces overcompensation of the friction ($F_f(x_2) > F_f(x_2 + x_3)$ for some time intervals), and, as a result, the system exhibits limit cycling around the desired state. The cause for this limit cycle is, therefore, directly related to the instability of the observer error. Note that for the numerical integration of the differential inclusion (8), we replaced both the friction model (2) and the friction compensation rule (5) with a switch model (see [19] for more details on this technique). Furthermore, for the applied parameter settings, (9) is not fulfilled and the solution in Fig. 6 is not guaranteed to be unique (see Appendix I).

V. Nonexact Friction Compensation

In practice, small friction modeling errors can not be avoided. Obviously, this also holds for the friction modeling of the one-link robot. The plausible effects of such inevitable modeling errors on the proposed friction compensation strategy are investigated in this section. This is done by introducing a scaled friction compensation law, as incorporated in (8) for $r \neq 1$. Obviously, in practice, modeling errors will not be of this form, but this type of scaling of the compensation law allows to investigate the effects of both overcompensation and undercompensation in a relatively straightforward manner.

The equilibria of (8) for $r \neq 1$ satisfy the same equations as for the case of exact friction compensation [see (12) and (13) and the inclusion $G_{ne}(x_2^*) \in [-F_s^-, F_s^+]$, where $G_{ne}(x) = (b + LJ)x + rF_f(x)$. Similarly to the case of exact friction compensation, the origin is always an equilibrium point (as desired). For the case of nonexact compensation, it holds that $\lim_{x\downarrow 0} G_{ne}(x) = rF_s^+$ and $\lim_{x\uparrow 0} G_{ne}(x) = -rF_s^-$. Consequently, an equilibrium set will exist for the case of undercompensation ($r < 1$), irrespectively of the value for L. As illustrated in Fig. 7, the value of L does influence the magnitude of the maximum steady-state positioning error for this case. This figure also indicates that friction compensation (even in the case of undercompensation) ensures a smaller steady-state positioning error than exists without compensation (see Fig. 4). Moreover, the controller parameters can be used to decrease the maximum steady-state position error even further in a similar manner as for the case of exact friction compen-

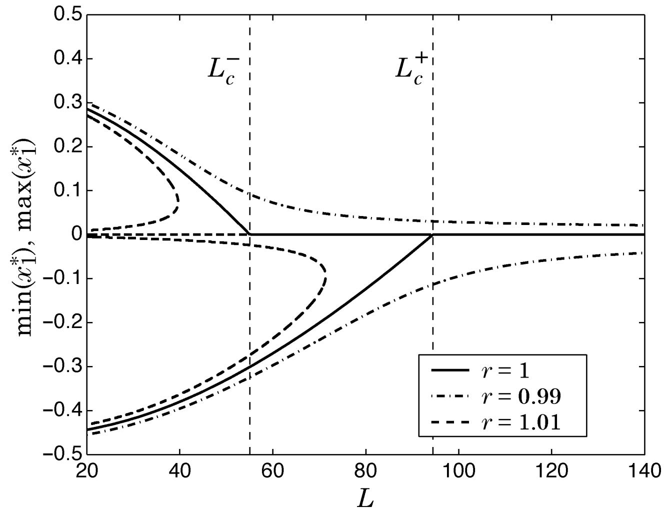

Fig. 7. Effect of the equilibrium set on the steady-state error in x_1 for $n_1 = 0.4$, $n_2 = 0.02$, and different values for r.

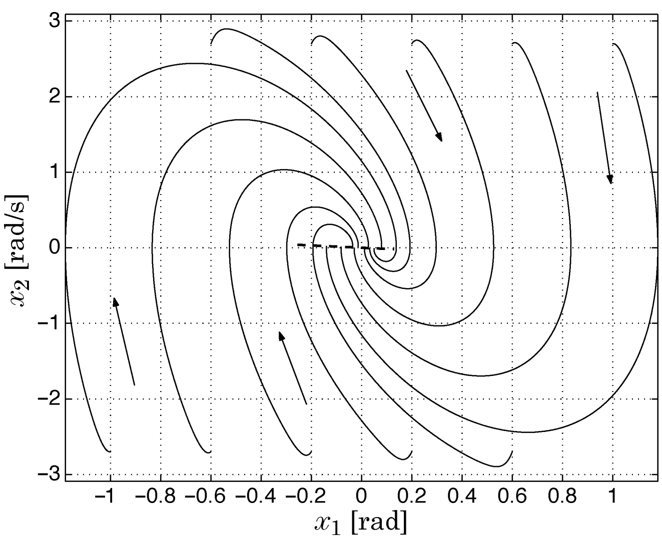

Fig. 8. Attractive equilibrium set (dashed line) for the case of undercompensation ($r = 0.95$), projected onto the plane $x_3 = 0$, for $n_1 = 0.4$, $n_2 = 0.02$, and $L = 95$.

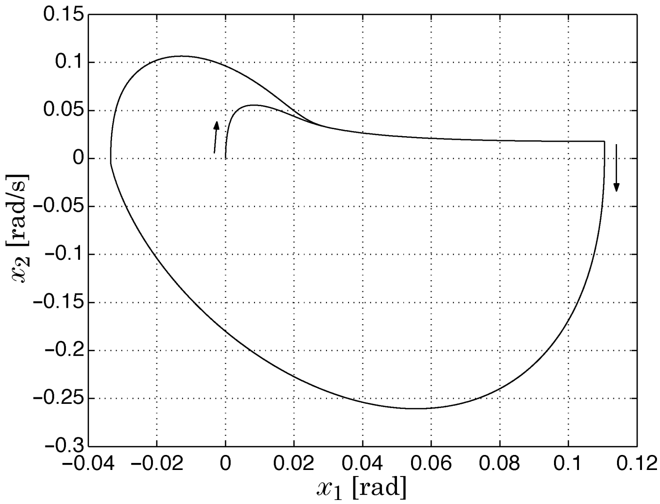

Fig. 9. Numerical solution for the case of overcompensation ($r = 1.01$), projected onto the plane $x_3 = 0$, with $\mathbf{x}(0) = 1 \cdot 10^{-6}[0, 1, 0]$, $n_1 = 0.4$, $n_2 = 0.02$, and $L = 95$.

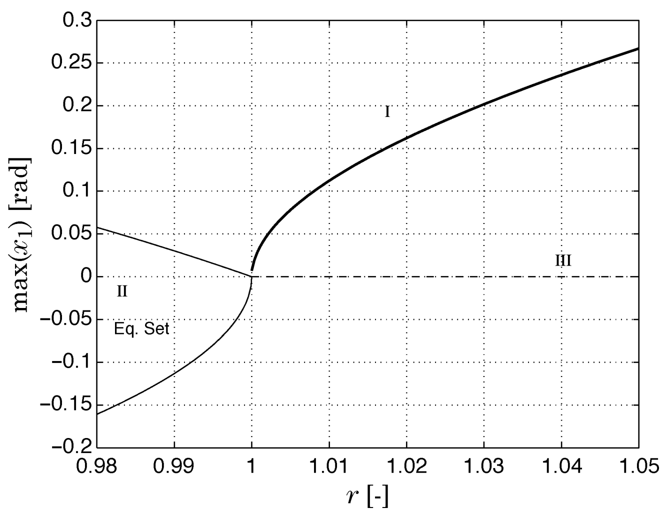

Fig. 10. Bifurcation diagram with bifurcation parameter r with $n_1 = 0.4$, $n_2 = 0.02, L = 95$ [(I) (stable) branch of limit cycles, (II) (stable) equilibrium set and (III) (unstable) equilibrium point].

sation (see Section IV-A). For the case of overcompensation ($r > 1$), an equilibrium set only exists for r very close to one; the equilibrium set rapidly shrinks to an isolated equilibrium point for increasing r.

The dynamics of (8) for $r \neq 1$ are numerically examined in more details. In Fig. 8, the result of this approach is depicted for the case of undercompensation ($r = 0.95$). All solutions tend to the equilibrium set and no other type of solutions, such as for example limit cycles, are observed in this case. A solution for the case of overcompensation ($r = 1.01$), with an initial condition taken very close to the origin, is depicted in Fig. 9. The latter figure indicates that, for the case of overcompensation, the origin of (8) is not stable anymore and the system exhibits limit cycling.

The branch of limit cycles for a varying value of r is traced using *pseudo arclength continuation* [23] in combination with the shooting method. The local stability of the limit cycles is determined by inspection of the Floquet multipliers. The resulting bifurcation diagram is shown in Fig. 10 for an observer gain $L = 95 > L_c$. A limit cycle is characterized in this figure by plotting the value of $\max(|x_1|)$ of the limit cycle. Clearly, the closed-loop system already exhibits stable limit cycling if the friction is only slightly overcompensated. For the case of undercompensation, a zero steady-state error is no longer guaranteed due to the existence of an equilibrium set. However, the system does not exhibit limit cycling in this case.

For the positioning task, the system must come at rest as close as possible to the desired position. Consequently, the possibility of limit cycling must be excluded. The case of undercompensation should, therefore, always be preferred over the case of overcompensation. To cope with small modeling errors, a relatively simple strategy is, therefore, to scale down the compensation rule until no more limit cycling behavior occurs. The dependency of the maximum steady-state error on the controller

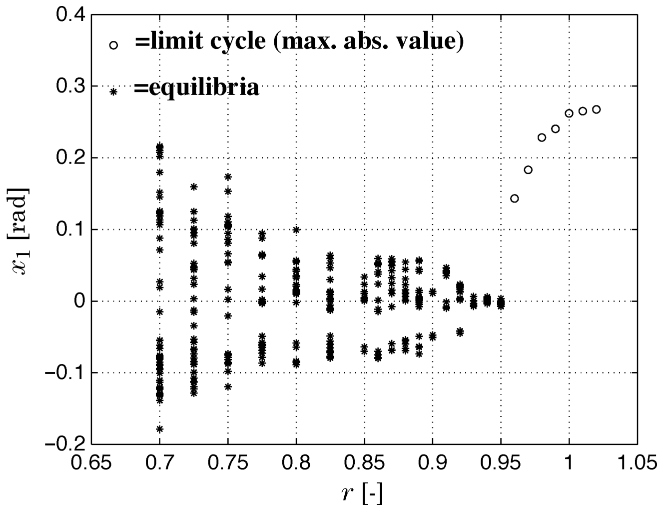

Fig. 11. Experimentally found bifurcation diagram with bifurcation parameter r and $n_1 = 0.4, n_2 = 0.02, L = 95$.

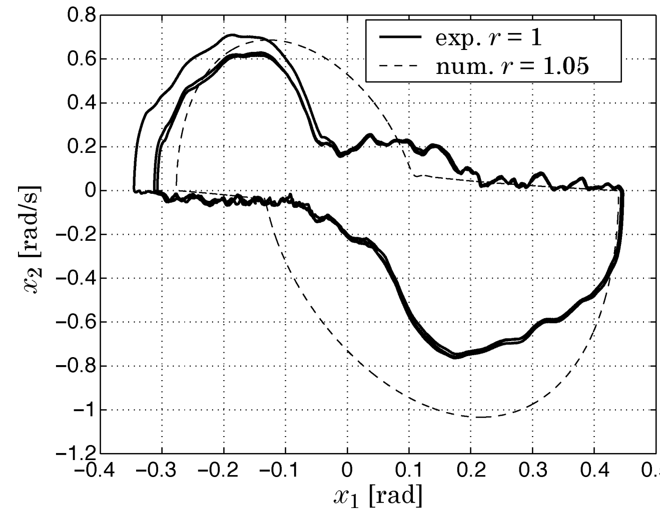

Fig. 12. Comparison of numerically obtained limit cycle for $r = 1.05$ with experimental results for $r = 1, n_1 = 0.4, n_2 = 0.02, L = 35 < L_c$.

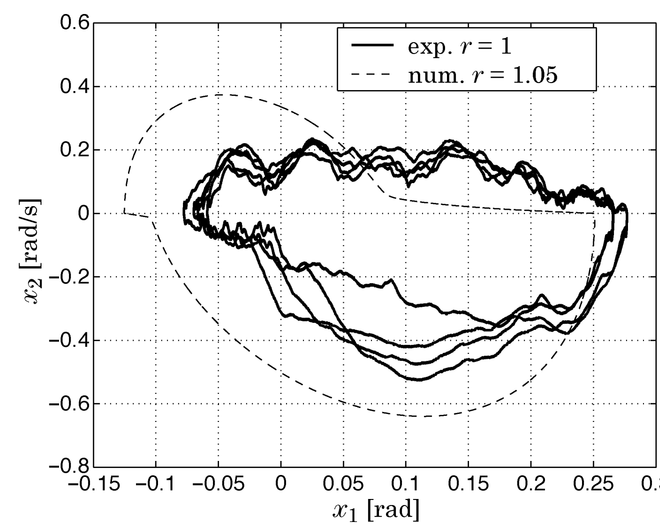

Fig. 13. Comparison of numerically obtained limit cycle for $r = 1.05$ with experimental results for $r = 1, n_1 = 0.4, n_2 = 0.02, L = 100 > L_c$.

and observer gain(s) is similar to those in the case of exact friction compensation. Consequently, the resulting steady-state positioning error for this case, can be reduced by increasing the observer gain and the proportional controller gain or by decreasing the derivative gain (see Section IV-A). Namely, the equilibrium set becomes smaller by taking these measures.

VI. Experimental Validation

In this section, the result of the previous sections are validated with experiments. For the experimental implementation, the modeling and identification of dry friction will never be exact. In Section V, the effects of small friction modeling errors for the reduced-order observer-based friction compensation is studied by simply scaling the friction compensation rule. For the experimental implementation, the error in the estimated friction is due to both identification errors and friction modeling errors and is, therefore, far more complicated than accounted for by simply scale the compensation model. Possibly, the effect of more complicated friction modeling errors (for example due to neglecting dynamical friction effects) may give different results. Therefore, the effectiveness of the scaling-down-approach of the friction compensation to avoid possible limit-cycling behavior will also be tested at the experimental implementation. Furthermore, the experimental results will be compared with the numerical results for the closed-loop system (8) with $r \neq 1$. At the experimental setup, the link of the robot is driven by an induction motor, which is powered by pulse width modulation (PWM). The real-time control of the setup is handled by a PC with a dSPACE [24] controller board. The angular displacement of the link is measured at the experimental setup with a resolution of $2 \cdot 10^4$ increments per revolution of the motor shaft. Due to the gear ratio of the transmission of 8.192 $[-]$, the effective resolution for the position of the link is $3.835 \cdot 10^{-5}$ rad.

A bifurcation diagram, with the scaling constant r as bifurcation parameter, involving experimental results is shown in Fig. 11. Herein, the stars $(^*)$ indicate equilibria and the circles (o) indicate limit cycles. Comparison of Figs. 10 and 11 reveals a clear qualitative correspondence. The bifurcation point in Fig. 11 is, of course, not located exactly at $r = 1$ since not only the friction compensation law is scaled but the real friction deviates from the friction model as well (for example due to dynamical friction effect). Moreover, the difference between the real friction and the friction model (the modeling error) is not of the form of a mere scaling. Nevertheless, the theoretical and experimental results agree to the extent that undercompensation leads to the existence of an equilibrium set (resulting in nonzero steady-state errors) and overcompensation leads to limit cycling. These observations are found for wide range of initial conditions.

Fig. 12 shows experimental results for $L < L_c$ and $r = 1$. Clearly, the system exhibits limit cycling around the desired position. In Fig. 12, a numerically obtained limit cycle for (8) with $r = 1.05$ is also shown. From the comparison, it can be noted that, although the projections do posses shape similarities, the experimental result does not exactly agree with the simulation result. However, the results do show qualitative similar behavior. In Fig. 13, similar results are depicted for $L > L_c$. For this higher observer gain value, the measured limit cycle has become more noisy, probably due the combination of unmodeled dynamics and the higher observer gain. Again, the results show

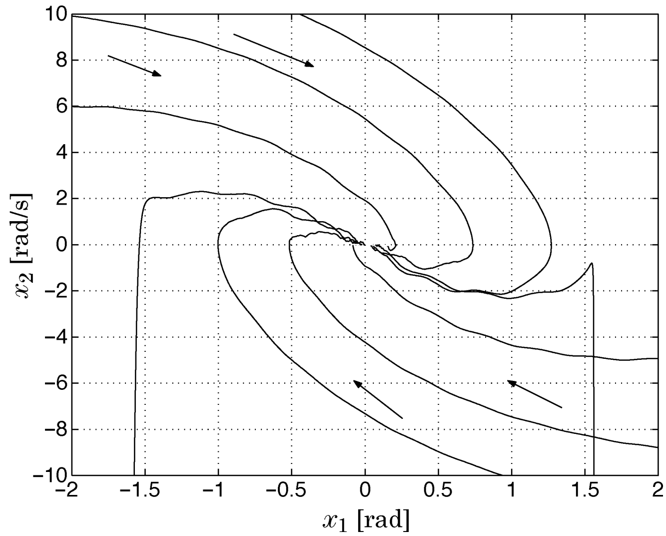

Fig. 14. Measured equilibrium set for $n_1 = 0.4$, $n_2 = 0.02$, $L = 95$, and $r = 0.8$.

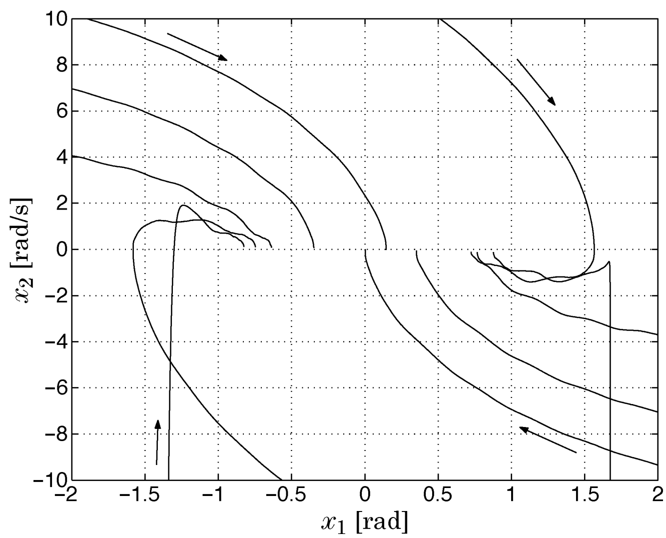

Fig. 15. Measured equilibrium set for $n_1 = 0.4$, $n_2 = 0.02$, $L = 95$, and $r = 0$ (no compensation).

a qualitative correspondence. For $r = 0.8$, the experimentally obtained equilibrium set is depicted in Fig. 14 and similarly for $r = 0$ (no compensation) in Fig. 15. Clearly, the use of proposed friction compensation, with undercompensation of the friction, does not guarantee a zero steady-state error. However, the use of the friction compensation strategy ensures, also for the experimental implementation, a large decrease in the size of the maximum steady-state error (i.e. $\max |x_1^*|_{r=0} = 0.87$ rad and $\max |x_1^*|_{r=0.8} = 0.15$ rad). Moreover, the experimental setup does not exhibit limit cycling if the friction is undercompensated. Consequently, assuring that the friction is not overcompensated, the use of the reduced-order, observer-based friction compensation at the experimental setup provides an increase in positioning performance without the existence of limit cycling behavior.

VII. Conclusion

A friction compensation strategy for a PD controlled one-link robot using a reduced-order observer is proposed. Based on experiments, a set-valued friction model is identified to support a model-based friction compensation approach. Since only position measurements are available and the friction depends on velocity, a reduced-order observer is used to provide velocity estimates. Both the cases of exact friction compensation and nonexact friction compensation are studied. In the case of exact friction compensation, it is shown that the observer gain is critical for the stability of the equilibrium point coinciding with the set-point. An analytical expression for the critical observer gain is derived. If the observer gain is taken larger than this critical value, it is shown that the set-point is a globally exponentially stable equilibrium point for arbitrary positive controller gains. Clearly, the mild condition on the controller gains in combination with the derived critical observer gain can be considered as a design rule for the closed-loop system. Moreover, for an observer gain taken lower than this critical value, an equilibrium set exists and limit cycling can occur (both undesired phenomena for the position performance). In the case of nonexact friction compensation, it is shown that undercompensation of the friction leads to a significant increase in positioning performance. However, a zero steady-state error can not be guaranteed in this case, due to the existence of an equilibrium set. If the friction is overcompensated the system exhibits limit cycling. These results are obtained both in simulation and experiments. Consequently, it is advised to choose for a small level of undercompensation instead of a small level of overcompensation when exact friction compensation is not possible.

The stability analysis of the closed-loop system is performed by studying the closed-loop system in a cascade structure or to be more precise by separating the (nonlinear) observer error dynamics and the system dynamics. This approach can easily be extended for controllers other that the PD controller as considered in this paper, and may be applied to other observer-based friction compensated systems. However, for the case of nonexact friction compensation, an additional integral interaction in the controller may provide robustness against steady-state errors but may also lead to additional instabilities. This matter and extension of the results toward friction compensated multi-degree-of-freedom systems with both full-order and reduced-order observers are topics for further research.

Appendix I
Uniqueness of Solutions

In this appendix, uniqueness of solutions for (8) is examined. With the friction model (2) and the compensation rule (5) incorporated in (8), two surfaces of discontinuity (commonly termed as switch surfaces) exist in the state-space of (8). For the study on the uniqueness of solutions of (8), the dynamics close to these two switch surfaces will be investigated. The switch surface in the state space of (8) related to the discontinuity in the friction model is denoted by Σ_1 and is indicated by $h_1(\mathbf{x}) = x_2 + x_3 = 0$. The switch plane related to the discontinuity in the friction compensation rule is denoted by Σ_2 and is indicated by $h_2(\mathbf{x}) = x_2 = 0$. The dynamics close to a switch plane Σ_i are studied by examining the projections of the vector field on the corresponding normal, evaluated infinitely close to Σ_i. The vector field evaluated infinitely close to Σ_i in the subspace where $h_i(\mathbf{x}) < 0$ is denoted by $\mathbf{f}^-(\mathbf{x})$ and similarly for $h_i(\mathbf{x}) > 0$ by $\mathbf{f}^+(\mathbf{x})$.

First, the dynamics near Σ_1, with corresponding normal $\mathbf{n}_1 = [0, 1, 1]^T$, are examined. The projections of the vector field on $\mathbf{n}_1$, evaluated infinitely close to Σ_1 are $\mathbf{n}_1^T\mathbf{f}^-(\mathbf{x}) = (1/J)(u_c + rF_f(x_2) + F_s^-)$ and $\mathbf{n}_1^T\mathbf{f}^+(\mathbf{x}) = (1/J)(u_c + rF_f(x_2) - F_s^+)$, where u_c is the controller torque as defined in (4). A solution will intersect Σ_1 transversally if $(\mathbf{n}_1^T\mathbf{f}^-(\mathbf{x}))(\mathbf{n}_1^T\mathbf{f}^+(\mathbf{x})) > 0$ and, consequently, if $u_c + rF_f(x_2) < F_s^-$ or $u_c + rF_f(x_2) > F_s^+$. Attracting sliding modes appear if $\mathbf{n}_1^T\mathbf{f}^-(\mathbf{x}) > 0$ and $\mathbf{n}_1^T\mathbf{f}^+(\mathbf{x}) < 0$ and, consequently, if $-F_s^- < u_c + rF_f(x_2) < F_s^+$. Moreover, repulsive sliding modes appear if $\mathbf{n}_1^T\mathbf{f}^-(\mathbf{x}) < 0$ and $\mathbf{n}_1^T\mathbf{f}^+(\mathbf{x}) > 0$. Since this would require $u_c + rF_f(x_2) + F_s^- < 0$ and $u_c + rF_f(x_2) - F_s^+ > 0$, no repulsive sliding modes along Σ_1 can occur.

Next, the dynamics near Σ_2 are examined. Since only the second component of the normal vector to Σ_2 is nonzero: $\mathbf{n}_2 = [0, 1, 0]^T$, and only the third component of the right-hand side of (8) is discontinuous, the projection of the vector field on $\mathbf{n}_2$, evaluated infinitely close to the switch surface Σ_2 is continuous and equals $\mathbf{n}_2^T\mathbf{f}^-(\mathbf{x}) = \mathbf{n}_2^T\mathbf{f}^+(\mathbf{x}) = Lx_3 - (n_1/J)x_1$. Solutions are, therefore, always transversal to the switch plane Σ_2, except on the line

$$\Gamma = \left\{ \boldsymbol{x} \in \Sigma_2 | Lx_3 - \frac{n_1}{J}x_1 = 0 \right\}. \tag{18}$$

Namely, on the line defined by (18), the situation occurs that $\mathbf{n}_2^T\mathbf{f}^-(\mathbf{x}) = \mathbf{n}_2^T\mathbf{f}^+(\mathbf{x}) = 0$, since the vector field is locally parallel to Σ_2 at this line. The point $x_3 = 0$ on Γ reflects the origin in the state-space of (8) and is an equilibrium point of (8) (see Sections IV and V). Therefore, the discontinuity related to the friction model is not taken into account in the following. In order to understand the dynamics of (8) on Γ, one should realize that on Γ the vector field is set valued. The vector field is locally parallel to Σ_2 at Γ and solutions may slide along Γ. However, sliding along Γ is only possible if the direction of Γ lays in the convex hull of the set-valued vector field $\alpha\mathbf{p}_\Gamma \in \mathbf{f}(\mathbf{x})|_{\mathbf{x}\in\Gamma}$, where $\alpha \in \mathbb{R}$ and

$$\mathbf{p}_\Gamma = \begin{bmatrix} \frac{JL}{n_1} & 0 & 1 \end{bmatrix}^T \tag{19}$$

as illustrated in Fig. 16. Since solutions which slide along Γ are also allowed to leave Γ (and, consequently, Σ_2), by choosing any other direction from the convex hull of the set-valued vector field, this type of solution is not unique. Consequently, to guarantee uniqueness of solutions of (8), sliding along Γ must be avoided. In order to study possible sliding modes along Γ, we introduce a vector $\mathbf{n}_\Gamma = [-(n_1/JL)\ 0\ 1]^T$ in the plane Σ_2 which is normal to $\mathbf{p}_\Gamma$. A condition such that sliding along Γ is impossible is $(\mathbf{n}_\Gamma^T\mathbf{f}(\mathbf{x}(t)))(\mathbf{n}_\Gamma^T\mathbf{f}(\mathbf{x}(t))) > 0\ \forall\, \mathbf{x} \in \Gamma$, since this assures that $\alpha\mathbf{p}_\Gamma \notin \mathbf{f}(\mathbf{x})|_{\mathbf{x}\in\Gamma}$. Consequently, sliding along Γ is not possible if $(1/J^2)(K(x_3) - r[-F_s^-, F_s^+])(K(x_3) - r[-F_s^-, F_s^+]) > 0$, where $K(x) = (b + LJ + (n_1/L))x + F_f(x)$. Since it hold that $\lim_{x_3\downarrow 0} K(x_3) = F_s^+$ and $\lim_{x_3\uparrow 0} K(x_3) = F_s^-$, a sufficient condition such that no sliding modes along Γ

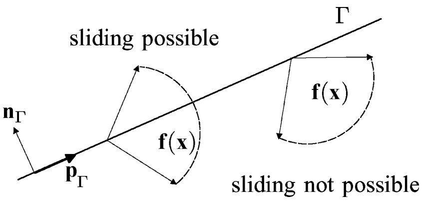

Fig. 16. Possible sliding mode due to the set-valued vector field.

can occur for $r \leq 1$ is that the function $K(x_3)$ is strictly increasing for all $x_3 \neq 0$. This is attained if $(\partial/\partial x_3)K(x_3) > 0\ \forall\, x_3 \neq 0$ and, consequently, if

$$L + \frac{n_1}{L} > \frac{1}{J}(-\lambda - b) \tag{20}$$

where λ is defined by (10). Clearly, solutions of (8) are not automatically guaranteed to be unique. However, for the case $r \leq 1$, a sufficient condition is derived such that uniqueness of solutions of (8) is guaranteed. It is noted that $L > L_c$ (see Section IV), is sufficient to satisfy (20) for arbitrary $n_1 > 0$. The presented sufficient condition for the uniqueness of solutions for (8) ensures that no sliding modes along Σ_2 [(the switch plane related to the discontinuity in the compensation rule (5)] can exist. Consequently, the solution of (8) is not influenced by which exact value of the friction compensation torque is taken from the set $r[-F_s^-, F_s^+]$. This property is beneficial for implementation purposes.

REFERENCES

[1] B. Armstrong-Hélourvy, *Control of Machines With Friction*. New York: Kluwer, 1991.

[2] B. Armstrong-Hélourvy, P. Dupont, and C. Canudas de Wit, "A survey of models, analysis tools and compensation methods for the control of machines with friction," *Automatica*, vol. 30, no. 7, pp. 1083–1138, 1994.

[3] R. H. A. Hensen, "Controlled Mechanical Systems With Friction," Ph.D. dissertation, Dept. Mech. Eng., Eindhoven Univ. Technol., Eindhoven, The Netherlands, 2002.

[4] C. J. Radcliffe and S. C. Southward, "A property of stick-slip friction models which promotes limit cycle generation," in *Proc. American Control Conf.*, San Diego, CA, 1990, pp. 1198–1203.

[5] S. L. Ipri and H. Asada, "Tuned dither for friction suppression during force-guided robotic assembly," in *Proc. IEEE/RSJ Int. Conf. Intelligent Robots and Systems*, vol. 1, 1995, pp. 310–315.

[6] C. T. Johnson and R. D. Lorenz, "Experimental identification of friction and its compensation in precise, position controlled mechanisms," *IEEE Trans. Ind. Appl.*, vol. 28, no. 6, pp. 1392–1398, Nov./Dec. 1992.

[7] C. Canudas de Wit, H. Olsson, K. J. Åström, and P. Lischinsky, "A new model for control of systems with friction," *IEEE Trans. Autom. Control*, vol. 40, no. 3, pp. 419–425, Mar. 1995.

[8] J. Swevers, F. Al-Bender, C. Ganseman, and T. Prajogo, "An integrated friction model structure with improved presliding behavior for accurate friction compensation," *IEEE Trans. Autom. Control*, vol. 45, no. 4, pp. 675–686, Apr. 2000.

[9] H. Olsson, K. J. Åström, C. Canudas de Wit, M. Gäfvert, and P. Lischinsky, "Friction models and friction compensations," *Eur. J. Contr.*, vol. 4, no. 3, pp. 176–195, 1998.

[10] C. Canudas de Wit, P. Noel, A. Aubin, B. Brogliato, and P. Drevet, "Adaptive friction compensation in robot manipulators: Low velocities," in *Proc. IEEE Int. Conf. Robotics and Automation*, vol. 3, 1989, pp. 1352–1357.

[11] S. C. Southward, C. J. Radcliffe, and C. R. MacCluer, "Robust nonlinear stick-slip friction compensation," *J. Dyn. Syst., Meas., Contr.*, vol. 113, pp. 639–644, 1991.

[12] B. Friedland and S. Mentzelopoulou, "On adaptive friction compensation without velocity measurement," in *Proc. 1st IEEE Conf. Control Applications*, Dayton, OH, 1992, pp. 1076–1081.

[13] D. Putra and H. Nijmeijer, "Limit cycling in observer-based controlled mechanical systems with friction: numerical analysis and experimental validation," *Int. J. Bif. Chaos*, vol. 14, no. 9, pp. 3083–3093, 2004.
[14] D. G. Luenberger, "An introduction to observers," *IEEE Trans. Autom. Control*, vol. AC-16, no. 6, pp. 596–602, Jun. 1971.
[15] F. Altpeter, "Friction Modeling, Identification and Compensation," Ph.D. dissertation, Dept. Genie Mech., Ecole Polytech. Fed. Lausanne, Lausanne, Switzerland, 1999.
[16] M. Iwasaki and N. Matsui, "Observer-based nonlinear friction compensation in servo drive system," in *Proc. 4th Int. Workshop Advanced Motion ContrOL*, Tsu-City, Japan, 1996, pp. 344–348.
[17] E. G. Papadopoulos and G. C. Chasparis, "Analysis and model-based control of servomechanisms with friction," in *Proc. IEEE/RSJ Int. Conf. Intelligent Robots Systems*, vol. 3, 2002, pp. 2109–2114.
[18] G. F. Franklin, D. A. Powell, and A. Emami-Naeini, *Feedback Control of Dynamic Systems*, 3rd ed. Reading, MA: Addison-Wesley, 1994.
[19] R. I. Leine and H. Nijmeijer, *Dynamics and Bifurcations in Non-Smooth Mechanical Systems*. New York: Springer-Verlag, 2004, vol. 18, Lecture Notes Appl. Comput. Mech.
[20] A. F. Filippov, *Differential Equations With Discontinuous Right-Hand Sides*. Dordrecht, The Netherlands: Kluwer, 1988.
[21] H. K. Khalil, *Nonlinear Systems*. Englewood Cliffs, NJ: Prentice-Hall, 1996.
[22] D. Shevitz and B. Paden, "Lyapunov stability theory of nonsmooth systems," *IEEE Trans. Autom. Control*, vol. 39, no. 9, pp. 1910–1914, Sep. 1994.
[23] T. S. Parker and L. O. Chua, *Practical Numerical Algorithms for Chaotic Systems*. New York: Springer-Verlag, 1989.
[24] *DS1102 User's Guide. dSPACE Digital Signal Processing and Control Engineering GmbH*, 1999.